Molecular dynamics calculations for low-energy helium atoms on a nickel surface

1989 J. Phys.: Condens. Matter 1 10021

(http://iopscience.iop.org/0953-8984/1/50/005)

J. Phys.: Condens. Matter **1** (1989) 10021–10037. Printed in the UK

Molecular dynamics calculations for low-energy helium atoms on a nickel surface

V Rosato†§, G Maino‡ and A Ventura‡

† Comitato Nazionale per l'Energia Nucleare e le Energie Alternative, Dipartimento Tecnologie Intersettoriali di Base, Divisione Materiali, Centro Ricerche Casaccia, CP 2400 Roma, Italy

‡ Comitato Nazionale per l'Energia Nucleare e le Energie Alternative, Viale Ercolani 8, Bologna, Italy

Received 28 November 1988, in final form 2 June 1989

Abstract. We have reproduced, by means of molecular dynamics simulations, the behaviour of helium atoms impinging on a nickel {100} surface at finite temperature ($T = 0.3T_m$, where T_m is the bulk melting temperature) with incident energies ranging from 0.1 to 50 eV. We have evaluated the reflection coefficients as a function of incident energy for given incidence angle, $\alpha = 0°$. Several reflection mechanisms have been individuated in the higher-energy range ($10 \leqslant E_{in} \leqslant 50$ eV). Furthermore, we discuss the role of the thermal spike associated with displacement cascades in the process of creation of surface defects. We describe the structural modifications induced on the metal lattice by the simultaneous presence of helium atoms and lattice point defects. The evaluation of the energies required to form these defective configurations confirms the strong tendency of helium to migrate to defective regions rather than to defect-free ones.

1. Introduction

In tokamaks with high-temperature plasmas the first wall is subject to a flux of light ions ($\simeq 10^{19}$–10^{22} ions cm^{-2} s^{-1}) with a probable energy spectrum ranging from 1 to 100 eV [1]. Evaluation of the mechanical effects induced by the presence of those species in the metal structure is one of the main tasks in the development of fusion reactor materials.

Several mechanisms are responsible for the presence of light ions and atoms in structural materials, among them the implantation of particles in a direct interaction of plasma with exposed surfaces and their production in the bulk region through neutron-induced reactions.

The case of helium is of major significance: the observed growth of helium bubbles and their segregation into lattice defects, such as grain boundaries and dislocations, lead ultimately to severe embrittlement [2], blistering and swelling [3], with consequent loss of mechanical properties of the irradiated materials.

An important area in the research and development of materials deals with the selection of the basic physical phenomena which are at the origin of these observed macroscopic events [4–7]. Although the technological significance of these studies

§ ENEA contract No 2760.

0953-8984/89/5010021 + 17 $02.50

resides mainly in the development of structural steels, a first step in singling out the fundamental processes of radiation damage consists in the study of elementary effects in pure metals: as often pointed out, simple metals reproduce, at least qualitatively, the complex behaviour of structural steels; for instance, strong analogies in the diffusive behaviour of nickel atoms in nickel and in austenitic alloys have been underlined [8].

The present work can be divided into two parts. First, we discuss the problem of the interaction of low-energy helium ions ($E_{in} \leqslant 50$ eV) with the metal surface and we analyse the modifications induced on the surface structure and the behaviour of reflected, or absorbed, projectiles. In the second part, we deal with the modifications induced in the bulk structure of the metal, originating from the lattice relaxation around the guest atoms and their interactions with pre-existent point defects.

As far as ion back-scattering is concerned, experimental data are available mainly for incident energies $E_{in} > 1$ keV (see [1] and references therein). The lack of experimental information in the low-energy range has not allowed, up to now, a complete comprehension of the atomic-scale processes which govern sputtering, surface erosion and ion reflection.

The most widespread numerical approach used to tackle irradiation problems is the binary collision (BC) model [9], where the real-space trajectories of incident ions and displaced lattice atoms are determined from a sequence of two-body collisions which begins at the time of the primary knock-on and finishes when the kinetic energy of each atom involved in the displacement cascades turns out to be smaller than the phenomenological value of the corresponding activation energy for diffusion.

A great amount of work has been carried out in the energy range above 100 eV using BC codes, among others MARLOWE [9] and TRIM [10, 11], in order to study the behaviour of reflected projectiles and the characteristics of sputtered atoms for a wide class of projectile–target combinations. The results have been used mainly to understand the structure of experimental energy spectra and to single out the atomic-scale contributions of different scattering phenomena [12].

The applicability of BC codes breaks down, however, at low incident energies ($E_{in} \leqslant 100$ eV). In this energy range, which is important in the plasma device scenario, many-body interactions are no longer negligible and have to be taken into account for a realistic modelling of scattering events: the system, metal lattice plus incident ions, has to be treated in a fully dynamical way, through the use of molecular dynamics (MD) codes. This approach is extremely general since it avoids several approximations typical of BC models, such as static lattice and indirect introduction of thermal motion, but, in turn, it can handle only small systems (a few thousand atoms) during very short time periods (picoseconds). The most important phenomena in irradiated materials occur, however, on an atomic scale and in times which are comparable [1] to the vibrational period of the lattice atoms (10^{-13}–10^{-12} s). Therefore the use of MD codes is fully legitimate.

As far as the behaviour of helium atoms in the bulk region is concerned, the basic statement of the problem is the vanishingly small equilibrium solubility of helium in metals. The closed-shell electronic configuration prevents helium, like other rare gases, from sharing electrons with metal atoms, thus inhibiting the formation of any kind of bond. This phenomenon induces a large strain field in the lattice in the neighbourhood of the helium atom, once it is located at some interstitial site. The intensity of the strain field is a measure of the heat of solubility, which is of the order of 3.5 eV in the case of helium in nickel [13].

The replacement of the interstitial helium atom with a pre-existent lattice vacancy cancels the strain field almost completely: therefore, the binding energy of the helium

atom with a vacancy, E^{B}_{He-V}, is of the same order of magnitude of the heat of solution ($E^{B}_{He-V} = 2.1$ eV [13]). The fact that the substitutional position for helium is energetically favourable with respect to the interstitial one originates a very efficient 'trapping' mechanism, exerted by lattice vacancies, which strongly affects the diffusive behaviour of helium atoms: in fact, they show a strong tendency to fill vacancies and form clusters. The migration energy of interstitial helium ($E^{M}_{i} = 0.1$ eV [13] $\div$ $E^{M}_{i} = 0.35$ eV [14]) has been found experimentally lower than that of substitutional helium, $E^{M}_{s} > 3$ eV [1]. Moreover, under certain conditions, helium atoms form clusters and self-trap by creating vacancy–interstitial Frenkel pairs, even in the absence of damage or thermal defects. As pointed out by Wilson *et al* [6], the collective action of even small clusters of helium atoms is sufficient for spontaneous creation of additional vacancies and associated self-interstitials: helium atoms can push lattice atoms off their normal sites and the latter find it energetically more convenient to remain in the vicinity of the cluster, thus creating 'near-Frenkel-pair' defects. This simple energetic picture at the atomistic scale makes it possible to understand some observed features like the high concentration of substitutional helium with respect to the interstitial one [13] and the nucleation of helium bubbles in irradiated materials [1].

In spite of many suggestions on migration mechanisms, a clear quantitative measure of the activation energy for diffusion has not been given yet [1]. The interpretation of diffusion data in terms of simple interstitial migration over macroscopic distances has been implemented by introducing the effect of a 'trapping–detrapping' mechanism with thermal and non-thermal vacancies [15]. Furthermore, bulk diffusion does not seem to be influenced by extended lattice defects like grain boundaries: similar activation energies for diffusion have been found for single crystals and polycrystals [15]. Helium is permanently trapped in the lattice structure, either in the form of gas-filled voids, or solid clusters merged into the grains or segregated along grain boundaries and dislocations [1, 2]. Even at high temperatures, $T = 0.8T_m$, where T_m is the bulk melting temperature, only a small percentage of implanted helium is desorbed from the surfaces.

The main purpose of this work is to give a representative atomic-scale description of the phenomena induced by the presence of helium atoms on the surrounding host lattice and to describe the most important dynamical properties of both species. For this purpose we have used the MD technique, which is a very powerful tool to investigate the thermodynamical and structural properties of materials [16, 17]. Recently, interesting results have been obtained by means of MD codes in the study of hydrogen on metals. In particular, the MD approach has emphasised the drastic reduction of the particle reflection coefficient at low incident energy, $E_{in} < 3$ eV, due to hydrogen capture into particular surface sites [18].

Using a MD model developed in reference [19], we have studied the reflection properties of low-energy helium atoms scattered by a {100} nickel surface at low temperature, $T = 0.3T_m$. This temperature has been chosen for a number of reasons: (i) it allows quantitative reproduction of the thermodynamical behaviour of the lattice [19]; (ii) it mimics a temperature scale which is supposed to be important in controlled fusion devices; (iii) thermodynamical equilibrium conditions can be imposed without taking into account high-temperature surface effects, like roughening and premelting.

The MD reproduction of the microscopic behaviour of lattice atoms allows us to analyse the surface effects induced by temperature variations due to scattering events. Therefore, we have studied the possible correlations between defect creation and onset of local structural transitions on the surface, i.e. solid–liquid or roughening, induced by the incident flux, by measuring the local temperature of each atomic layer of the model during the scattering events.

Table 1. Cohesive energy parameters.

β (eV)	q	A (eV)	p
1.7557	2.70	0.1368	10.0

Finally, we have evaluated the dynamical response of the bulk structure (in terms of relaxation) due to the presence of helium atoms and to their interaction with bulk-lattice defects.

2. Computational model

We recall in this section the main features of the adopted MD model, which has been described in more detail elsewhere [19, 20].

It has been shown [21] that several characteristics of FCC d-band transition metals depend only on the width of the electronic density of states, i.e. on the second moment (SM) of its distribution. According to a tight-binding scheme, the cohesive energy of the metal has been divided into an attractive part, derived in the framework of a SM approximation, and a repulsive pairwise interaction. The total cohesive energy, E_{coh}, can thus be written:

$$E_{coh} = -\sum_i \left[-\left(\sum_j \beta^2 \exp(-2q(r_{ij}/r_0 - 1)) \right)^{1/2} + \sum_j A \exp(-p(r_{ij}/r_0 - 1)) \right] \tag{1}$$

where β is an effective hopping integral, r_{ij} the distance between atoms i and j and r_0 the first-neighbour distance. The parameter q gives the distance dependence of the hopping integral. The parameters A, β, q and p have been determined by fitting the experimental cohesive energy, the lattice parameter, the bulk modulus and the shear elastic constants under the equilibrium condition of vanishing hydrostatic pressure and are given in table 1. Metal–metal interactions are limited to first neighbours: the non-pairwise nature of the attractive interaction, however, allows us to extend the real interaction up to the first shell of neighbours of the first neighbours.

The helium–metal interaction is described by a fully repulsive potential

$$V(r) = \Gamma \exp(-\gamma r)/r \tag{2}$$

where r is the distance between the helium projectile and a lattice atom. The potential parameters have been determined by Melius *et al* [22]: $\Gamma = 45.9$ eV Å and $\gamma = 2.03$ Å^{-1} in the He–Ni interaction. We have imposed a cut-off interaction radius, $R_c = 3.5$ Å; this value allows us to take into account first and second He neighbours, once the helium atom is in the equilibrium interstitial octahedral site (O_h). Potential (2) can only describe elastic collisions of helium with lattice atoms; the so called inelastic energy losses due to the interactions with the electron gas filling the solid have been found to be of minor importance compared with the elastic losses for the present case and are not explicitly included in this simulation. A few figures of comparison between nuclear and electronic stopping powers will be given in a subsequent section.

The physical system used in the present simulation is an assembly of $N = 1800$ atoms arranged in a FCC structure of 25 {100} atomic planes parallel to the free surface, each

containing 72 atoms. Periodic boundary conditions (PBC) along the directions parallel to the surface have been imposed, with a period equal to the lattice size, i.e. six lattice parameters. Along the ⟨100⟩ direction perpendicular to the surface PBC have been imposed with a period of 25 lattice parameters, twice the lattice size in that direction, so as to describe the presence of free space above and below the system [20]. This free space should contain surface defects (adatoms which will be detected at a distance from the surface equal to half a lattice parameter) and atoms promoted to the vapour phase (detected at a distance greater than the cut-off radius R_c), which ensure thermodynamic equilibrium at a given temperature. The appropriateness of such PBC has been proved elsewhere [23].

The model size has been chosen so as to reproduce correctly the thermodynamic and structural surface properties, like the mean-square amplitude of the atomic vibrations and relaxation of the uppermost atomic planes. It has already been pointed out, in fact, that correct reproduction of these properties in a system with free surfaces can be achieved only if interactions between surfaces are avoided, i.e. if a reasonable part of the system reproduces the thermodynamic properties of the bulk lattice [23]. Furthermore, the necessity of simulating absorption events requires a sample thick enough to explore incident energies up to $E_{in} > 50$ eV.

Another reason for the choice of a thick sample is related to the increase of lattice temperature in the case of complete release of projectile energy. Small systems cannot afford to absorb impacts at $E_{in} = 50$ eV, because they would produce a temperature increase driving the whole system to a solid–liquid transition.

The Newton equations of motion for the system have been solved under the constraints of the microcanonical ensemble (total energy, volume and particle number are constants of motion) by using the central difference algorithm with a time step $h = 3 \times 10^{-16}$ s. This value has been chosen in order to obtain total energy conservation with an accuracy better than 10^{-4} even in the case of high-energy impacts.

Initially, the metal lattice has been thermalised at the desired temperature, $T = 500\ \text{K} \simeq 0.3T_m$, in about 2×10^4 steps. During this period several physical quantities have been monitored in order to ensure a final thermalised state with realistic values of lattice parameter, surface relaxation and mean-square amplitude of atomic vibrations. The quantitative agreement between the thermodynamic and structural properties predicted by the model and the corresponding experimental data has been proved to be quite satisfactory [19].

The introduction through the thermalisation procedure of spurious longitudinal waves in the direction perpendicular to the surface has been avoided by the method described in references [20] and [23].

At the beginning of the MD simulation, the helium atom is placed at a fixed distance from the surface, z_0, slightly greater than R_c, and the x_0 and y_0 on the initial plane are taken at random. For a given incident energy 100 particle histories have been simulated with different (x_0, y_0) choices in order to explore a wide class of possible impact conditions and to obtain significant statistics. In all cases the initial velocity is perpendicular to the surface, with zenith angle $\alpha = 0°$.

The system, consisting of 1800 lattice atoms and one helium projectile, is then left free to evolve and the equations of motion iteratively integrated up to the onset of one of the following events, which stops the computer run: (i) the projectile is reflected and reaches a distance from the surface greater than the cut-off radius, R_c: at this point the projectile kinetic energy is recorded, together with the velocity components, and the scattering angle with respect to the surface normal is evaluated; (ii) the projectile is

Table 2. Particle and energy reflection coefficients.

E_{in} (eV)	C_N (%)	C_E (%)
0.1	100.0	93.5
1.0	100.0	80.3
10.0	88.0	52.0
30.0	50.0	33.0
50.0	44.0	28.8

absorbed and its kinetic energy decreases to the order of magnitude of the He migration energy, E_{He}^{M}, whose experimental value is about 0.35 eV in nickel [14]. In this case, the potential energy of helium inside the lattice characterises the particular interstitial site where it has been trapped.

In all cases the total duration of a simulation has never exceeded 3000 time steps, i.e. 9×10^{-13} s, indicating that fast processes govern both slowing down of absorbed projectiles and back-scattering events. During this period no other helium atoms have been sent on the surface. Since the exposed area is about 400 $Å^2$ the simulated flux does not exceed $\Phi = 2.5 \times 10^{25}$ ions $cm^{-2} s^{-1}$.

The final positions of the lattice atoms have been recorded and analysed in order to study the processes of defect creation in the bulk and on the surface. The relevant results are shown in the following sections. In particular, § 3 is devoted to the analysis of back-scattered particles, whose behaviour is important for the problem of 'recycling' [24]. Section 4 contains the analysis of surface defects; § 5 describes the behaviour of helium in the bulk structure; finally, § 6 summarises the results of the present calculations and compares them with available experimental data.

3. Back-scattering events

The main characteristics of the reflected beam are described in table 2, which gives particle and energy reflection coefficients, C_N and C_E respectively, against incident energy, E_{in}. C_N is defined by the ratio of the number of reflected particles, N_R, to the number of incident projectiles, N_T, and C_E is the ratio of the reflected energy, E_R, to the total energy sent on the surface, E_T:

$$C_N(E_{in}) = N_R/N_T \tag{3}$$

$$C_E(E_{in}) = E_R/E_T. \tag{4}$$

The analysis at very low E_{in} ($\simeq K_B T$), performed on the basis of the distributions of reflected energies at given E_{in}, in figures 1(*a*)–(*d*) shows that the projectile can exchange with the target an amount of energy which is comparable to the energy of a single lattice phonon: in fact, the histogram of reflected energies at $E_{in} = 0.1$ eV reveals the presence of important contributions to back-scattering up to $E_{out} = 1.7\ E_{in}$, which corresponds to an absorbed phonon of frequency of about 7 THz, not far from the main phonon peak of nickel at that temperature [19]. In the same figure (1(*a*)) the reflected energy distribution is shown not only for $T = 500$ K but also for $T = 0$ K; in the latter case the distribution consists of a main peak at $E_{out}/E_{in} = 0.936$ and, or course, an energy gain in back-scattering is no longer possible.

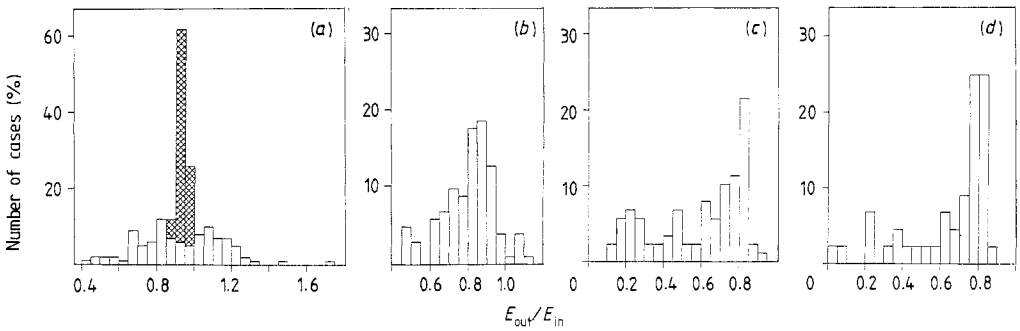

Figure 1. Energy distributions of reflected helium at various incident energies: (*a*) 0.1 eV, (*b*) 1.0 eV, (*c*) 10 eV, (*d*) 50 eV. Abscissae in units of E_{in}, ordinates in units of total number of reflected particles at given E, temperature $T = 500$ K, In (*a*) the hatched histogram is the reflected energy distribution at $E_{in} = 0.1$ eV, $T = 0$ K.

At higher energy ($10\text{ eV} \leqslant E_{in} \leqslant 50\text{ eV}$) the reflection coefficients decrease monotonically with increasing E_{in}. This trend is in reasonable agreement with low-energy extrapolation of numerical simulations based on BC model [1]; however, the MD results are systematically lower than the BC ones in the same energy range. This fact can be interpreted in terms of the target reaction to the guest atom, taken into account in MD models, consisting of a lattice relaxation around the projectile path, which makes its penetration easier. In a BC model, where lattice atoms cannot move if not directly involved in a scattering event, the target is 'stiffer' with respect to the interaction with the guest atom. Moreover, in a BC code, once a lattice atom has been displaced by the projectile, it can hardly restore its initial position. This leads to an overestimate of the number of created defects. Such a limitation has been taken over by MD models, where the introduction of a real thermal motion allows for an eventual recombination of unstable Frenkel pairs. In any case, the lattice relaxation around the projectile path is not observable when $E_{in} < 10$ eV, because the projectile energy is too low to induce the lattice reaction. Therefore, in this energy range, the qualifying difference between MD and BC codes does not play a crucial role for this particular effect.

Another interesting feature, typical of the higher-energy impacts, is the possibility of occurrence of two types of reflection processes: (i) direct reflection, when the projectile interacts with a few atoms of the first, or second, layer and is then back-scattered; (ii) delayed reflection, when the projectile penetrates much deeper into the solid (up to 20 atomic layers in the case $E_{in} = 50$ eV), diffuses freely with high kinetic energy in the layers below the surface and is subsequently desorbed through the surface, after a 'residence' time which can be up to 100 times longer than the typical direct reflection time at the same initial energy. In order to display this absorption–desorption mechanism, the real-space trajectory of the helium atom during one of these events, at $E_{in} = 30$ eV, is represented in figure 2 within the field of lattice atom positions as they are at the end of the helium trajectory. Bulk defects, created in multiple interactions before back-scattering, have already undergone recombination, while, on the surface, adatoms created by a local increase of temperature are clearly visible.

In the case of deep penetration into the solid it is possible to evaluate a trajectory-averaged energy loss per unit path length, due to elastic collisions of helium with lattice atoms; at $E_{in} = 30$ eV, for instance, we obtain $-\langle dE/ds\rangle_{el} = 0.65\text{ eV Å}^{-1}$ and the

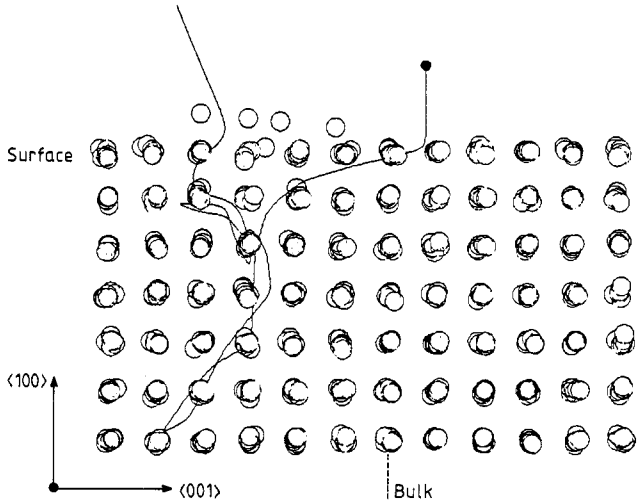

Figure 2. Delayed reflection, illustrated by the real-space trajectory of a helium atom with $E_{in} = 30$ eV during 1400 time steps in the field of a projection (along a ⟨100⟩ direction) of the first seven layers of the sample (view from one side). The presence of adatoms on the surface is noteworthy.

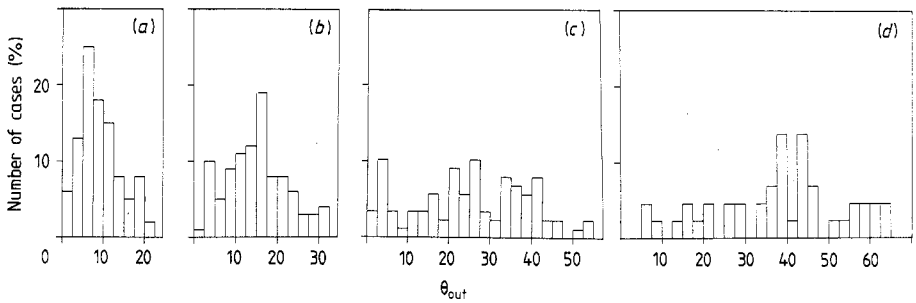

Figure 3. Angular distributions of reflected helium at the same E_{in} values as in figure 1. θ_{out} is the zenith angle with respect to the surface normal; $T = 500$ K.

average path length $\langle s \rangle = 46$ Å for projectiles undergoing absorption, or delayed reflection. An upper limit to the inelastic energy losses can be estimated in the framework of a jellium model for the solid, with the assumption that the projectile travels in a fully ionised state, by the method of reference [25], giving $-\langle dE/ds \rangle_{inel} = 0.39$ eV Å^{-1} over the same path length. The importance of the inelastic energy loss is even smaller at smaller E, since it is proportional to $\sqrt{E}$: that is why we have neglected inelastic effects in the present simulation.

Further qualitative information on back-scattering can be obtained from the angular distributions of reflected particles at given initial energy and incidence angle, as shown in figures 3(*a*)–(*d*). Although no direct correlation appears between exchanged energy and reflection angle, θ, the above-mentioned distributions show that the average reflection angle, θ, increases with increasing E_{in}. This corresponds to the naive picture of single collisions for low incident energies and multiple collisions for high energies. In

the latter case any correlation between initial and final projectile directions is lost. Figure 2 gives a clear illustration of this effect.

4. Creation of surface defects

As far as radiation damage is concerned, interesting results can be obtained from the analysis of defects created in the lattice by projectile interactions, either in the bulk or on the surface.

For the incident energy range of interest in the present work a straightforward calculation shows that the formation of stable Frenkel pairs in the bulk is quite unlikely. In the approximation of two-atom head-on collisions the maximum transferred energy is

$$K_{max} = 4m_1m_2E_{in}/(m_1 + m_2)^2 \tag{5}$$

where m_1 and m_2 are the masses of projectile and target, respectively, and E_{in} the incident kinetic energy [26]. K_{max} can be evaluated in the limiting cases of two-body collisions ($m_2 = m_{Ni}$) and simultaneous interaction with four surface atoms ($m_2 = 4m_{Ni}$ in FCC surface geometry), obtaining the lower and upper limits 3.3 eV and 11.9 eV for E_{in} = 50 eV. This energy range has to be compared with the formation energy of a bulk self-interstitial in its stable relaxed configuration (⟨100⟩ dumbbell), $E_{Si}^F = 3.55$ eV, as predicted by the model [19].

We have observed several cases where bulk lattice atoms have been strongly displaced by direct interactions with the projectile; the resulting Frenkel pairs, however, appear to be unstable, in the sense that they undergo recombination when the temperature of the system is quenched to 0 K.

We have also observed some examples of 'channelled' projectiles along the main crystallographic directions. In figure 4, for instance, the helium atom at $E_{in} = 50$ eV reaches the 13th layer below the surface without significant energy loss (less than $0.25E_{in}$). In this case the energy has been spent against a reaction force which originates from the presence of lattice atoms along the ⟨100⟩ channel.

The surface exposed to the flux of helium atoms is, of course, the most severely damaged part of the lattice. The analysis of the simulated events shows the presence of several sources of radiation damage. Surface atoms appear to be strongly displaced in consequence of three main processes: (i) direct impact with the projectile (primary knock-on (PKO)); on the compact faces with low Miller indexes a PKO takes place, in general, in the first few atomic layers, although one can have canalisation of the projectiles which interact, in that case, well below the surface; (ii) impact with PKO atoms, i.e. atoms directly displaced by the projectile; (iii) increase of local surface temperature, induced by thermalisation of the energy gained by the lattice during the collisions (thermal spike).

Since $K_BT \simeq 4 \times 10^{-2}$ eV, it results that $E_{in} \gg K_BT$ for the whole energy range considered in the present work. At $E_{in} = 50$ eV and maximum energy transfer, K_{max}, the corresponding temperature increase of the lattice is $\Delta T_{max} = 215$ K. Although the global temperature increase cannot exceed ΔT_{max}, strong temperature fluctuations can be produced in a single atomic layer for periods of the order of 10^{-14}–10^{-13} s. This phenomenon causes, particularly on the surface, the creation of 'thermal' defects, i.e. adatom–vacancy Frenkel pairs, which establish new equilibrium conditions as the local temperature rises. These pairs do not necessarily recombine, since the thermal energy is

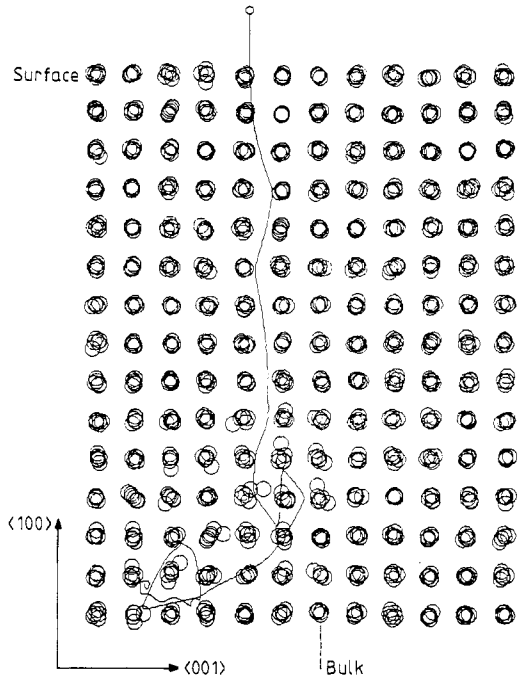

Figure 4. Channelled trajectory at E_{in} = 50 eV. Time duration and projection as in figure 2. The projectile goes through the first 15 layers from the surface and is finally absorbed.

rapidly shared with the other degrees of freedom. Stable defects could be produced because the diffusion enhanced by the thermal spike drives the dissociated defects into metastable lattice positions (interstitial or absorption sites), from which they cannot escape, due to the low thermal energy established on the surface at the regained thermodynamic equilibrium. This point can be easily understood by looking at the situation of figure 5, where a projectile with E_{in} = 30 eV impinges on the surface in the position indicated by the full circle (the view is from above the surface). In the same figure we have drawn the displacements of each atom of the first two atomic layers from $t = 0$ to $t = 1400$ time steps. It is worth noting (figure 2) that some surface atoms have been promoted, after strong displacements, to the vapour phase in the so called adatom layer. Since the projectile has been absorbed, the excitation responsible for the creation of defects must have a thermal origin. In fact, the same displaced atoms are distant from the impact area, as figure 5 shows; therefore, they have not received a direct impulsion from the projectile. Moreover, the weak displacement field around the impact zone excludes any possibility of indirect energy transmission through PKO atoms. This feature, related to the presence of a thermal spike, can be directly analysed through the evaluation of the time evolution of the local temperature measured in each atomic layer, from the time of the impact up to the complete sample thermalisation.

We have defined the local temperature, $T_\sigma(t)$, of a generic layer, σ, as the average kinetic energy sampled on the atoms belonging to layer σ at a given time, without including the projectile contribution. Figure 6 shows the time evolution of the local temperature in the surface layer, $T_1(t)$. Soon after the impact, indicated by an arrow in figure 6, one observes an increase of temperature in the impact area, because the kinetic energy of the projectile is released through fast local processes (collisions). During the

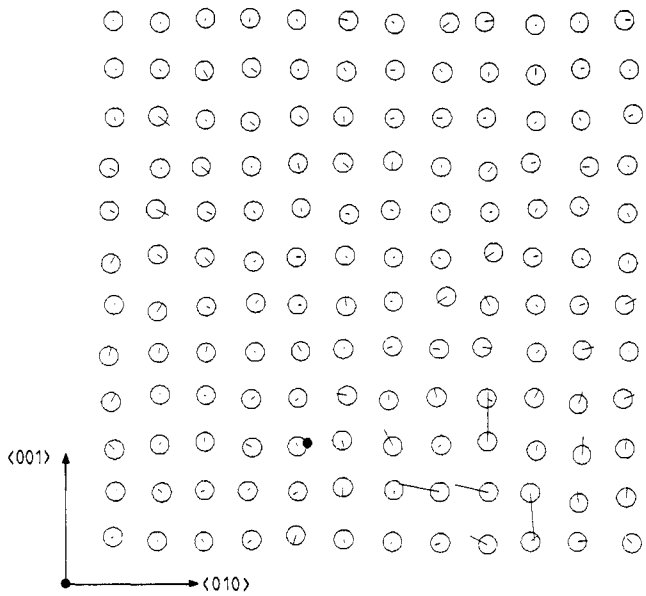

Figure 5. Displacements of the atoms belonging to the first two layers during the event of figure 2. Projection perpendicular to that of figure 2 (view from above the surface); time duration, 1400 steps. The long segments correspond to the displacements of adatoms in figure 2. The crystal axes are merely a guide to the eye.

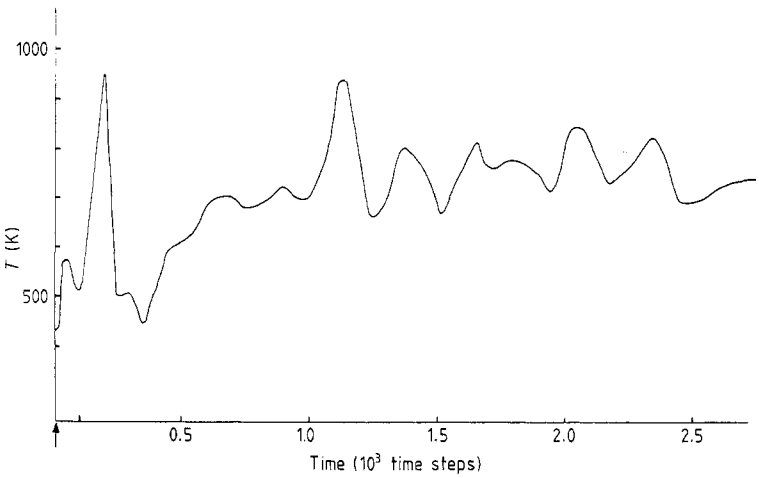

Figure 6. Time variation of the local temperature on the first atomic layer during a collisional event ending with absorption of the projectile. $E_{in} = 50$ eV.

spike, the local temperature grows up to 1000 K ($0.6T_m$) and exceeds the roughening temperature of that particular crystallographic face, which is of the order of 700 K [27]. In this case the temperature needed to create a step on the {100} face is of the order of 500 K per unit length, r_0. Therefore, a large number of defects is generated on the surface under the effect of the transition. These defects diffuse, with a diffusion coefficient

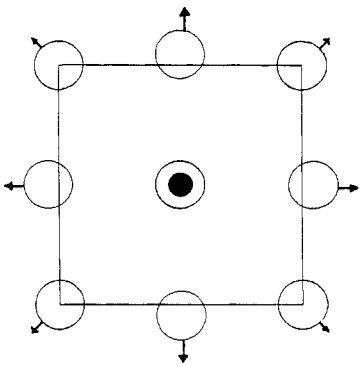

Figure 7. Equilibrium configuration of a helium atom in an O_h site at $T = 0$ K in a relaxed lattice configuration.

typical of a high-temperature regime. At a later time thermal equilibrium is restored with a net overall temperature increase corresponding to the kinetic energy released by the projectile to the lattice. One should also notice the time lag between projectile impact and onset of thermal spike, which gives a measure of the dynamical reaction time of the system.

5. Helium in bulk regions

We have studied the structural response of the nickel lattice to the presence of interstitial helium. After free diffusion in the lattice, the guest atom reduces its kinetic energy to a value smaller than the migration energy for an interstitial, $E^{M}_{He} = 0.35$ eV [14]. Then, the lattice is left free to relax around the helium atom, usually trapped in an O_h interstitial site, before quenching the entire system to $T = 0$ K in a few picoseconds. The potential energy in the relaxed configuration turns out to be $U^{rel}_{He}(O_h) = 3.12$ eV; in an O_h site of the unrelaxed lattice one would obtain $U^{unr}_{He}(O_h) = 4.62$ eV. The difference, $\Delta U = 1.50$ eV, gives rise to strong deformations in the unit lattice cell: the relative distance of the first neighbours of helium increases by a factor $\Delta d_1/d_1 = 0.092$ along the $\langle 100 \rangle$ direction, while the second neighbours are slightly displaced by $\Delta d_2/d_2 = 0.002$ along the $\langle 111 \rangle$ direction, as shown in figure 7.

In our simulation we have also placed the helium atom in the vicinity of a pre-existent point defect, like a vacancy or a self-interstitial, in order to study their mutual interaction. For example, the helium atom has been placed in an O_h site as a second neighbour of a lattice vacancy and its behaviour has been followed for the subsequent 10^4 time steps. After about 2×10^3 time steps spent oscillating around the initial site, the helium atom jumped, in a few hundred time steps, into the near vacancy, where it kept on vibrating around the new equilibrium configuration. Figure 8 shows the time dependence of the distance of helium from the initial O_h site, at $T = 700$ K ($\simeq 0.4 T_m$); here, the jump of one lattice spacing into the vacancy is clearly visible. It is worth noting that the mean-square amplitude of the helium oscillations in the substitutional site is twice as big as that in the interstitial O_h site at the same temperature, $\langle U^2_{He}(O_h) \rangle = 0.068$ Å^2. The helium potential energy in the relaxed substitutional position, obtained by quenching the system to 0 K as usual, is estimated to be U^{rel}_{He} (substitutional) = 1.36 eV, in comparison with the unrelaxed value, U^{unr}_{He} (substitutional) = 1.47 eV. This energy difference accounts for the small lattice distortion around helium in this configuration.

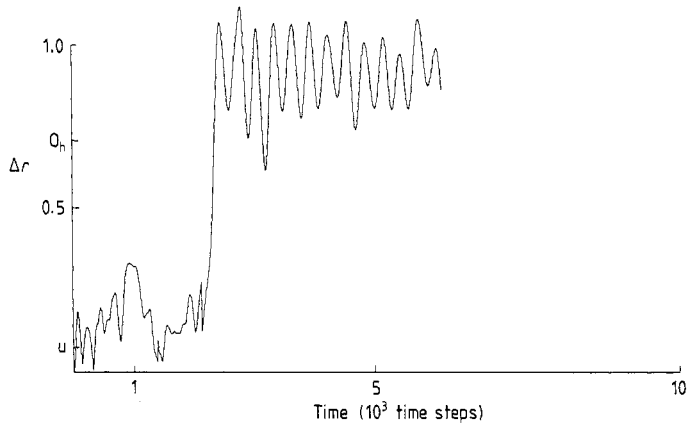

Figure 8. Distance Δr of the instantaneous position of helium from the initial O_h position as a function of time. In this case the helium atom has been placed in the vicinity of a pre-existent lattice vacancy. Crystal temperature $T = 700$ K.

As an example of interaction with self-interstitials, a helium and a nickel atom have been placed in the second neighbour's position as O_h interstitials inside contiguous unit cells, at $T = 700$ K. Then the system evolves during some 10^4 time steps at that temperature, and is subsequently quenched to $T = 0$ K in order to find the configuration of minimum energy. We have repeated these operations starting from the same lattice configuration, but assigning different initial positions to the two extra atoms, tetrahedral sites, for instance.

The resulting final configuration at zero temperature appears to be independent of the initial state. We have found two different stable configurations to which the system evolves. In the first case (case (ã)) shown in figure 9(*a*), the helium atom remains in the initial O_h position, or evolves toward it if it is not initially there, while the interstitial nickel moves in a ⟨100⟩ direction up to the creation of a stable ⟨100⟩ dumbbell, whose axis contains the helium atom too. In this case, the lattice relaxation around He in O_h fits the requirements for lattice relaxation around the dumbbell. In fact, the first neighbour of helium (atom A in figure 9(*a*)) moves toward the dumbbell, as required for the relaxation process around the dumbbell. In such a configuration we obtain $U_{He}^{(\tilde{a})} = 3.05$ eV.

The second allowed configuration (case (b̃)) is sketched in figure 9(*b*). Here, the helium atom migrates from the O_h site into a 'quasi' edge site characterised by coordination $C = 14$. In its displacement, it pushes a Ni first neighbour out of its initial position: in figure 9(*b*), the relative displacement of atom A is about 0.21. The interstitial nickel creates a ⟨100⟩ dumbbell, whose axis does not contain the helium atom. In case (b̃) the helium potential energy is somewhat lower than in case (ã), since $U_{He}^{(\tilde{b})} = 2.42$ eV. Nevertheless, the resulting local structure is strongly perturbed by the combined action of the two extra atoms.

The energy, E_F, required to form a given defective configuration containing a helium atom can be estimated as follows:

$$E_F = U_{He+D} - (U_{He} + U_D) \tag{6}$$

where U_{He+D} is the energy of the system containing helium and the defect, U_{He} is the

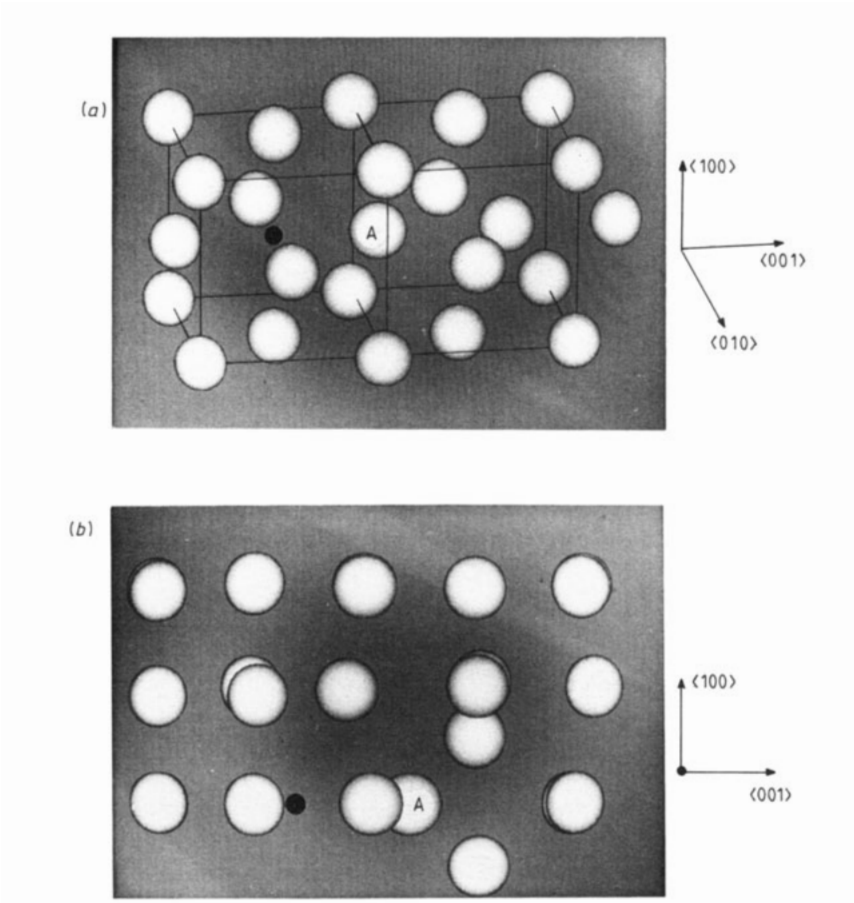

Figure 9. Stable equilibrium configurations, cases (ã) in figure 9(*a*) and (b̃) in figure 9(*b*), of helium interacting with a self-interstitial, see text for explanation.

energy of the system containing only the helium atom and U_D is the energy of the defective metal structure in the absence of helium. Equation (6) can be rewritten as follows:

$$E_F = [\langle {}^{He}U_M^{N\pm1}/(N\pm1)\rangle N + U_{He}^{N\pm1}] - [\langle {}^{0}U_M^{N\pm1}/(N\pm1)\rangle N + U_{He}^{N}] \tag{7}$$

where $\langle U_\alpha^N\rangle$ represents the α potential energy (α = M for metal and α = He for helium) in configurations $(N-1)$ (with vacancy), N (defect free), $(N+1)$ (with self-interstitial). The left-hand superscripts He and 0 refer to the presence or absence of helium, respectively. U_{He}^N is the He potential energy in configuration N. For the cases we have considered, $E_F(N)$ is the formation energy for a configuration where helium is in a defect-free zone, $E_F(N-1)$ for He in a substitutional position, $E_F(N+1)$ for He bound to a dumbbell in cases (ã) and (b̃), and we have obtained: $E_F(N) = 5.18$ eV, $E_F(N+1, (\tilde{a})) = 5.12$ eV, $E_F(N+1, (\tilde{b})) = 5.26$ eV, $E_F(N-1) = 2.73$ eV. From these results the helium–vacancy interaction energy can be obtained:

$$E(\text{He–V}) = E_F(N) - E_F(N-1) = 2.45\ \text{eV}. \tag{8}$$

This result can be compared with the values in the literature: E(He–V) = 2.1 eV [13], 3.2 eV [28] and 2.3–3.2 eV [14].

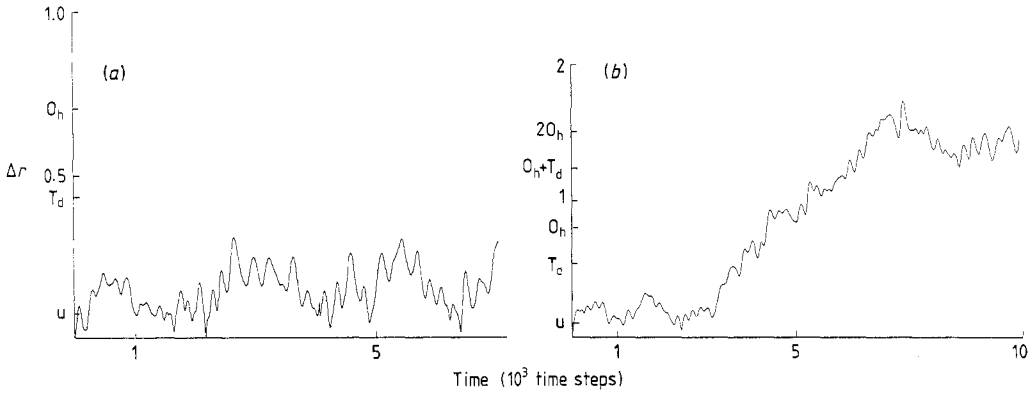

Figure 10. Time dependence of helium distance, Δr, from initial O_h site. Δr is expressed in units of the lattice parameter, time in units of 1000 time steps. (*a*) $T = 700$ K, (*b*) $T = 1100$ K. In (*b*) the distances of the nearest interstitial sites from the initial O_h position are marked on the ordinate axis: T_d is the tetrahedral site.

In addition, we have investigated the dynamical behaviour in the metal lattice at finite temperature for helium as a simple interstitial, or in the neighbourhood of a pre-existent vacancy. Although the short duration of the trajectories does not allow a definite evaluation of the diffusion coefficient, we have calculated the mean-square displacement of helium in different sites, or roughly estimated the migration energy for interstitial helium. Therefore, we have initially introduced the helium atom as an interstitial into an O_h site of a relaxed lattice configuration at two different temperatures, $T = 700$ K ($K_B T \simeq 0.06$ eV) and $T = 1100$ K ($K_B T \simeq 0.095$ eV). We have then followed the trajectory of the guest atom during the subsequent 10 000 time steps. As a result, the time variation of the distance, Δr, of helium from its initial O_h position is shown in figures 10(*a*) and (*b*) at $T = 700$ K and 1100 K, respectively. At $T = 700$ K the atom oscillates around the site with $\langle U^2_{He} \rangle = 0.068$ Å^2, to be compared with the mean-square amplitude of the lattice atom vibrations, $\langle U^2_{Ni} \rangle = 0.011$ Å^2. At $T = 1100$ K, on the contrary, after a short oscillation time around the initial site, with $\langle U^2_{He} \rangle = 0.093$ Å^2, the atom diffuses and its motion is illustrated in figure 10(*b*), where the geometrical distances of the main interstitial positions from the initial O_h site are also reported. The helium atom appears to diffuse almost freely, despite short residence periods, less than 10^{-15}–10^{-14} s, in temporary equilibrium positions which coincide with the nearest interstitial sites. Since the diffusion of interstitial helium occurs in the 700–1100 K temperature range, these extrema provide the lower and upper bounds of the migration energy, namely $0.060 < E^M_{He} < 0.095$ eV. The latter value is in agreement with the experimental lower limit of E^M_i, 0.1 eV [13].

6. Conclusions

Using the MD approach, we have simulated the behaviour of a {100} nickel surface irradiated with helium in the energy range from 0.1 to 50 eV for fixed incidence angle ($\alpha = 0°$) and crystal temperature ($T = 0.3 T_m$).

The interactions among the atoms of the model system have been derived in the framework of a tight-binding scheme, which reproduces correctly the thermodynamic and structural properties of FCC d-band transition metals [19].

We have studied the reflection properties of helium and found a super-elastic behaviour of the surface at $E_{in} \simeq K_B T$. The reflection coefficients decrease monotonically with increasing E_{in} and turn out systematically lower than the BC results for $E_{in} > 10$ eV. This difference could be attributed to the excessive stiffness of the simulated lattice in the BC approximation. Furthermore, we have stressed the existence of a process of delayed reflection at high E_{in}; in this case the projectile can create defects in layers well below the surface before back-scattering.

Different mechanisms responsible for the creation of surface Frenkel pairs have been analysed: the effect of the thermal spike seems to be the most important of them at $E_{in} > 10$ eV. The surface defects can hardly recombine, because the temperature variations restoring the thermodynamic equilibrium are extremely fast.

Although the incident energies are too low for the creation of stable bulk defects, we have evaluated the total formation energies of simple defective configurations containing a helium atom plus a vacancy, or a self-interstitial. The calculations support a strong 'chemical' bond between helium and lattice vacancies (E(He–V) = 2.45 eV). We have observed, moreover, a smaller, but significant, value for the interaction energy of helium and a self-interstitial dumbbell in configuration (ã) (E(He–D(ã)) = 0.06 eV).

These values indicate a tendency of helium to migrate into defective zones rather than into defect-free areas. Finally, the combined effect of helium and self-interstitials on lattice structure determines an important decrease of local order.

Various improvements and applications of the present model are in progress, in order to deal with other types of metal, e.g. BCC crystals; the explicit introduction of inelastic energy losses allows an extension to different projectiles, such as protons, at higher incident energies, for a better comparison with BC calculations.

Acknowledgments

One of us (VR) gratefully acknowledges valuable discussions with Drs A Barbu and B Legrand (Saclay), B Singh (Risø), Professors M Gillan (Keele) and B Brunelli (ENEA Frascati). Dr D Manco has contributed with his skill in computer graphics and Dr M Guillopé (Saclay) with enlightening discussions and critical reading of the manuscript.

References

[1] Behrish R and Eckstein W 1986 *Physics of Plasma-Wall Interactions in Controlled Fusion* ed. D E Post and R Behrish (New York: Plenum) pp 413–38
[2] Ullmaier H 1986 *Radiat. Eff.* **101** 147
[3] Erents S K and McCraken G M 1973 *Radiat. Eff.* **18** 191
[4] Lucas A A 1984 *Physica* B **127** 225
[5] Jung P and Schroeder H 1988 *J. Nucl. Mater.* **155–157** 1137
[6] Wilson W D, Bisson C L and Baskes M I 1981 *Phys. Rev.* B **24** 5616
[7] Marochov N, Perryman L J and Goodhew P J 1987 *J. Nucl. Mater.* **149** 296
[8] Müller A, Naundorf V and Macht M P 1988 *J. Nucl. Mater.* **155–157** 1128
[9] Robinson M T and Torrens I M 1974 *Phys. Rev.* B **9** 5008
[10] Biersack J P and Haggmark L G 1980 *Nucl. Instrum. Methods* **174** 257
[11] Biersack J P and Eckstein W 1984 *Appl. Phys.* A **34** 73

[12] Ghrayeb R, Purushotham M, Hou M and Bauer E 1987 *Phys. Rev.* B **36** 7364
[13] Sharafat S 1986 *PhD Thesis UCLA Report* ENG-8604 (Compilation of experimental data)
[14] Ullmaier H 1984 *Nucl. Fusion* **24** 1039
[15] Phillips V, Sonnenberg K and Williams J M 1982 *J. Nucl. Mater.* **107** 271
[16] Ciccotti G and Hoover W G (ed.) 1986 *Molecular Dynamics Simulations of Statistical Mechanical Systems* (Amsterdam: North-Holland)
[17] Jacucci G (ed.) 1986 *Computer Simulations in Physical Metallurgy* (Dordrecht: Reidel)
[18] Baskes M I 1984 *J. Nucl. Mater.* **128–129** 676
[19] Rosato V, Guillopé M and Legrand B 1989 *Phil. Mag.* A **59** 321
[20] Rosato V, Maino G and Ventura A 1989 *Comp. Phys. Commun.* **54** 251
[21] Ducastelle F 1970 *J. Physique* **31** 1055
[22] Melius C F, Bisson C L and Wilson W D 1978 *Phys. Rev.* B **18** 1647
[23] Rosato V, Ciccotti G and Pontikis V 1986 *Phys. Rev.* B **33** 1860
[24] Moller W and Roth J 1986 *Physics of Plasma-Wall Interactions in Controlled Fusion* ed. D E Post and R Behrish (New York: Plenum) pp 439–94
[25] Cherubini A and Ventura A 1985 *Lett. Nuovo Cimento* **44** 503
[26] Meyer O and Turos A 1987 *Mat. Sci. Rep.* **2** 371
[27] den Nijs M, Riedel E K, Conrad E H and Engel T 1985 *Phys. Rev. Lett.* **55** 1689
[28] Lewis M B 1987 *J. Nucl. Mater.* **149** 143